Joint inversion of seismic and electrical data in saturated porous media

Near Surface Geophysics

EAGE EUROPEAN ASSOCIATION OF GEOSCIENTISTS & ENGINEERS

*Near Surface Geophysics*, 2022, **20**, 64–81 doi: 10.1002/nsg.12184

# Joint inversion of seismic and electrical data in saturated porous media

Flora Garofalo[1*], Laura Valentina Socco[1] and Sebastiano Foti[2]

[1]*Politecnico di Torino - DIATI, C.so Duca degli Abruzzi, 24. 10129, Turin, Italy, and* [2]*Politecnico di Torino - DISEG, C.so Duca degli Abruzzi, 24. 10129, Turin, Italy*

Received July 2021, revision accepted October 2021

## ABSTRACT

Joint inversion strategies and physical constraints on model parameters may be used to mitigate equivalence problems caused by solution non-uniqueness. This strategy is quite a common practice in exploration geophysics, where dedicated rock physical studies are usually carried out, while it is not so frequent in near surface geophysics. We use porosity as a constraint among seismic wave velocities and electrical resistivity in a deterministic joint inversion algorithm for surface wave dispersion, P-wave traveltimes and apparent resistivity from vertical electrical sounding. These data are often available for near surface characterization. We show that the physical constraint among model parameters leads to internally consistent geophysical models in which solution non-uniqueness is mitigated. Moreover, an estimate of soil porosity is obtained as a relevant side product of the procedure. In particular, we consider a clean sand deposit and hence the appropriate formulations for the computation of porosity from seismic velocities and resistivity are implemented in the algorithm. We first demonstrate how the non-uniqueness of the solution is reduced in a synthetic case and then we applied the algorithm to a real-case study. The algorithm is here developed for one-dimensional condition and for granular soils to better investigate the physical constraint only, but it can be extended to the two-dimensional or three-dimensional case as well as to other materials with the adoption of proper rock physical relationships.

**Key words:** Inversion, Surface wave, Refraction, Electrical resistivity, Porosity.

## INTRODUCTION

Geophysical surveys typically require the solution of non-linear inverse problems that are ill-posed according to the Hadamard definition (1902). As a consequence, the reliability of the results is severely affected by solution non-uniqueness, that is, several possible solutions honour equally well the experimental data considering the data uncertainties (Backus & Gilbert, 1970). When different geophysical models are inverted separately, in the following this is termed 'individual' approach. A possible strategy to mitigate the consequences of solution non-uniqueness consists of joint inversion schemes, in which several data sets are simultaneously inverted to improve the reliability of the solution. Typically, these approaches require the combination of different geophysical models that can be solved by imposing the same structure of the subsurface. This is what in literature is called 'structural' joint inversion and helps to reduce the inconsistency of interfaces that could arise in the interpretation of the final models result from individual inversion (Dobróka *et al.*, 1991; Haber & Oldenburg, 1997; Gallardo & Meju, 2003, 2004; de Nardis *et al.*, 2005; Hu *et al.*, 2009; Doetsch *et al.*, 2010; Moorkamp *et al.*, 2011; Feng *et al.*, 2017; Senkaya *et al.*, 2020). A further step in joint inversion schemes is achieved by using rock physics relationships among the unknown geophysical model parameters to constrain themselves relative to each other in what is called

[*]Present address Eni S.p.A. - Natural Resources , Via Emilia 1, San Donato Milanese, Milano, 20097, Italy.
E-mail: flora.garofalo@eni.com

hereafter a 'physical' joint inversion. These *a priori* constraints ensure the convergence to a reliable and physically consistent subsurface model. Several examples of joint inversion are described in the literature, especially in the field of hydrocarbon exploration, where dedicated rock physics studies and characterization are carried out on the investigated formations and accurately calibrated empirical relationships among the geophysical parameters are available. An interesting review of joint inversion of seismic and electromagnetic data is provided by Moorkamp *et al.* (2016) and Colombo and Rovetta (2018). Among the hydrocarbon applications, one can find the scheme proposed by Gao *et al.* (2012), in which electromagnetic and seismic measurements are jointly inverted and the final model is solved for porosity and saturation degree, while the final geophysical parameter distributions, namely P-wave velocity and resistivity models, are calculated *a posteriori*. Dell'Aversana *et al.* (2011) proposed a joint inversion scheme for sonic, resistivity and density well-log data in order to derive rock porosity, fluid saturation and permeability. Gase *et al.* (2018) proposed a petrophysical model able to explain the effect of the dual porosity and water content on geophysical parameters in pyroclastic environment.

In near-surface geophysics, which does not benefit from the same abundance of dedicated rock-physics studies as for hydrocarbon exploration, the structural coupling only is more common (Hellman *et al.*, 2017; Ronczka *et al.*, 2018; Senkaya *et al.*, 2020) than the introduction of physical couplings between formations into inversion process. Some examples of physical joint inversion can be found in Dal Moro (2008) and Boiero and Socco (2014), who introduced the Poisson's ratio, which describes the deformation of a material in the perpendicular direction of the applied stress in terms of negative of the ratio between transverse strain and axial strain, as constraint between S-wave and P-wave velocities in a joint inversion of surface wave and P-wave refraction data. The joint inversion scheme proposed by Boiero and Socco (2014) was further extended by Garofalo *et al.* (2015) in order to include also electrical resistivity data imposing only a 'structural' joint inversion approach among seismic and electrical model parameters.

As far as the rock physics relationships are concerned, geomaterials can be modelled as a solid skeleton and the associated pores using the porous media theory. In a saturated porous medium, the properties of the pore fluid influence both seismic wave propagation and electrical current flow and hence, the porosity is a key property for both phenomena. A vast literature is available about the influence of the porosity on the S- and P- wave velocities as well as on the electrical resistivity. Biot (1956a,1956b) developed a seminal analytical study on seismic wave propagation in a fluid-saturated porous medium, while Wyllie *et al.* (1956, 1958) proposed an empirical study on the relationship between porosity and P-wave velocity. Based on these studies, several relationships between porosity and seismic velocities have been proposed, for example, Toksöz *et al.* (1976), Domenico (1984), Eberhart-Phillips *et al.* (1989), Berryman *et al.* (2002), and Foti *et al.* (2002). In addition, Mavko *et al.* (2009) provided a review of relationships among seismic velocity and porosity and the theoretical background for a suitable seismic analysis in porous media. Bruggeman (1935) before and Archie (1942) thereafter conducted empirical studies on the influence of the pore fluid on the electrical resistivity of saturated, or partially saturated, clean sands. Archie (1942) also introduced the tortuosity of the pore system as an additional parameter on top of the shape, size and packing of the grains. Waxman and Smits (1968) studied the influence of clay particles on the resistivity of the soil mixture. Later studies refined the relationship between the pore fluid properties and the resistivity of the mixture, for example, Jackson *et al.* (1978), Bussian (1983), de Lima (1995), Friedman (2005), Lesmes and Friedman (2005), Olsen (2011), and Kennedy and Herrick (2012).

Using these formulations, soil porosity can be estimated from geophysical surveys, rather than by direct estimation on laboratory samples, thus obtaining porosity for large volumes of the subsurface in natural conditions. Moreover, for uncemented coarse granular materials, common in the near surface, it is difficult to retrieve undisturbed samples without resorting to very expensive techniques, such as ground freezing (Singh *et al.*, 1982; Hofmann *et al.*, 2000) or gel-push sampler (Mori & Sakai, 2016). The abovementioned relationships may also be used to constrain seismic and electrical models, in the perspective of joint inversion of different data to mitigate the non-uniqueness of the solution as it is common in hydrocarbon exploration (Moorkamp *et al.*, 2016; Colombo & Rovetta, 2018).

In near-surface geophysics, the physical joint inversion between seismic and electromagnetic method is not so common because of a lack of rock-physics investigation and characterization. In the present work, we propose a physical joint inversion scheme of one-dimensional (1D) surface-wave dispersion, P-wave refraction and apparent resistivity data from vertical electrical sounding, to characterize a pack of sedimentary layers including clean sand formations. This is a situation quite common in the near surface as well as the adopted geophysical investigation methods. We constrain the P-wave and S-wave velocities through

the Poisson's ratio as suggested by Piatti *et al.* (2013), and we introduce a constraint between seismic velocities and resistivity through porosity. The paper is organized as follows: after a description of the inversion algorithm, a synthetic example and a case study are reported. Examples are provided for 1D models, but the proposed approach can be extended to those two-dimensional and three-dimensional inversion schemes based on spatially constrained local 1D models (Auken & Christiansen, 2004; Viezzoli *et al.*, 2008; Socco *et al.*, 2009; Boiero & Socco, 2014).

## METHOD

The proposed joint inversion algorithm combines seismic and resistivity data: surface-wave dispersion curves, P-wave travel times and apparent resistivity curves. The inversion algorithm is the same used by Garofalo *et al.* (2015) for two-dimensional data. We here adopt a simplified one-dimensional inversion scheme and introduce porosity as physical constraint among model parameters. A brief description of the inversion scheme follows, while further details are reported by Garofalo *et al.* (2015).

### Data, forward response and model parameters vectors

The dispersion of surface wave is represented by the dispersion curve ($\mathbf{dc}(f)$): phase velocity as a function of frequency $f$ with the associated uncertainties $\mathbf{e}_{\mathrm{obs,dc}}(f)$. The P-wave traveltimes ($\mathbf{pwt}(x)$) are represented by the first arrival of refracted P-waves as a function of the distance $x$ of the receivers from the source with the associated uncertainties $\mathbf{e}_{\mathrm{obs,pwt}}(x)$. The resistivity data are represented by the apparent resistivity curve ($\mathbf{ar}(es)$) with associated uncertainties $\mathbf{e}_{\mathrm{obs,ar}}(es)$ as a function of electrode spacing $es$ in the Schlumberger configuration of a vertical electrical sounding. Each data point of the vector $\mathbf{d}_{\mathrm{obs}}$ is hence characterized by its related uncertainties in the vector $\mathbf{e}_{\mathrm{obs}}$ that can result from a statistical analysis if the measurements were repeated sufficient times, otherwise it could be defined consistent with data sampling. The experimental data vector $\mathbf{d}_{\mathrm{obs}}$ and the associated covariance matrix $\mathbf{C}_{\mathrm{obs}}$ are hence:

$$\mathbf{d}_{\mathrm{obs}} = \left[\mathbf{dc}\left(f\right);\ \mathbf{pwt}\left(x\right);\ \mathbf{ar}\left(es\right)\right], \tag{1}$$

$$\mathbf{C}_{\mathrm{obs}} = \mathbf{cov}\left[\mathbf{e}_{\mathrm{obs,dc}}\left(f\right);\ \mathbf{e}_{\mathrm{obs,pwt}}\left(\mathbf{x}\right);\ \mathbf{e}_{\mathrm{obs,ar}}\left(es\right)\right]. \tag{2}$$

We assume a one-dimensional layered model with $l$ layers over a half space. The considered model parameters are S- and P-wave velocities ($V_{S,i}$ and $V_{P,i}$, respectively), resistivity ($R_i$) and the thickness ($h_i$) of each layer $i$, hence the model parameters vector is:

$$\mathbf{m} = \left[h_1; \ldots; h_l; V_{S,1}; \ldots; V_{S,l+1}; V_{P,1}; \ldots; V_{P,l+1}; R_1; \ldots; R_{l+1}\right]. \tag{3}$$

The forward response $g(\mathbf{m})$ is computed by adopting the Haskell (1953) and Thomson (1950) method for surface wave dispersion curves **dc** and it is mainly a function of $h_i$, $V_{S,i}$ and $V_{P,i}$. The forward model for P-wave traveltimes **pwt** is computed as function of $h_i$ and $V_{P,i}$ and it is based on the geometry of the refracted P-wave ray-paths in the case of horizontal planar layers model (Reynolds, 1997); while the Koefoed formulation (1979), which takes into account $h_i$ and $R_{,i}$, is adopted for apparent resistivity curves **ar**.

### The coupling factors

Despite each method investigating different properties of the subsurface, all of the experimental data are sensitive to interfaces and vertical heterogeneity. Thus, the layer thickness is the first coupling factor and this parameter is constrained by the three different data sets in the joint inversion scheme, assuming common interfaces for the different models. In other words, the thickness $h_i$ is solved by all the three data sets.

Poisson's ratio $\nu(\mathbf{m})$ is used to link $V_{S,i}$ and $V_{P,i}$ to each other. This coupling factor is introduced in the joint inversion algorithm by limiting the value of $\nu(\mathbf{m})$ between 0.0 and 0.5, that is, the physical acceptable range, and minimizing the difference of the value $\nu(\mathbf{m})$ with respect to a reference *a priori* value $\nu$. The strength of the latter is represented by the diagonal covariance matrix $\mathbf{C}_\nu$: the lower the value, the stronger the constraint and hence the algorithm forces the solution towards those values of $V_S$ and $V_P$ that meet the *a priori* Poisson value $\nu$. The values in the diagonal matrix $\mathbf{C}_\nu$ could vary from 0.001 to 1.000, from very strong to very weak constraints. For further information about this constraint, please refer to Piatti *et al.* (2013) and Boiero and Socco (2014).

Finally, we introduce the porosity as a further physical constraint between seismic velocities and resistivity. This constraint is implemented as the minimization at each iteration $n$th of the distance between the porosity $\phi_S$, associated to the seismic velocities $V_{S,n}$ and $V_{P,n}$, and the porosity $\phi_R$ associated to the resistivity $R_n$. We studied the specific case of saturated granular material and a discussion about this follows. However, the formulations of $\phi_S$ and $\phi_R$, which must be implemented in the inversion algorithm, depend on the material

properties and hence these should be evaluated as the more suitable for the investigated site. Since the constraint on porosity requires the assumption of realistic petrophysical relationships between porosity and seismic velocities and porosity and resistivity, it can be applied only for those layers where the expected geological conditions can be reliably assumed or an empirical site relationship is known. The length of vectors $\phi_S$ and $\phi_R$ is equal to the number of layers in which the constraint is applied. For example, if the constraint is applied only in one layer (as in our synthetic and real case studies), $\phi_S$ and $\phi_R$ reduce to scalars. This constraint is tuned by the diagonal covariance matrix $\mathbf{C}_\phi$, built as the square of the error assumed between the two porosity estimations. If porosity is expressed as decimals, then the diagonal values of $\mathbf{C}_\phi$ could vary between 0.001, very strong, and 1.000, very weak constraints.

### The inversion algorithm

The overall misfit function $Q$ is defined as

$$\begin{aligned} Q = &\left[(\mathbf{d}_{\text{obs}} - g(\mathbf{m}))^T \mathbf{C}_{\text{obs}}^{-1} (\mathbf{d}_{\text{obs}} - g(\mathbf{m}))\right] \\ &+ \left[(\mathbf{m}_{\text{P}} - \mathbf{m})^{\text{T}} \mathbf{C}_{\text{P}}^{-1} (\mathbf{m}_{\text{P}} - \mathbf{m})\right] \\ &+ \left[(\boldsymbol{\nu} - \boldsymbol{\nu}(\mathbf{m}))^{\text{T}} \mathbf{C}_{\nu}^{-1} (\boldsymbol{\nu} - \boldsymbol{\nu}(\mathbf{m}))\right] \\ &+ \left[(\phi_R(\mathbf{m}) - \phi_S(\mathbf{m}))^T \mathbf{C}_{\phi}^{-1} (\phi_R(\mathbf{m}) - \phi_S(\mathbf{m}))\right], \end{aligned} \tag{4}$$

The vector $\mathbf{m}_{\text{P}}$ contains the reference *a priori* model and the corresponding uncertainties are expressed by the covariance matrix $\mathbf{C}_{\text{P}}$.

The misfit function is then minimized using a quasi-Newton damped least-square method (Tarantola, 1987; Aster *et al.*, 2005), leading to an iterative algorithm in which the model $\mathbf{m}_{\text{n}}$ at the $n$th iteration is updated in $\mathbf{m}_{\text{n+1}}$, according to:

$$\begin{aligned} \mathbf{m}_{\text{n+1}} = \mathbf{m}_{\text{n}} + &\left( \begin{bmatrix} \mathbf{G}^{\text{T}} \mathbf{C}_{\text{obs}}^{-1} G \\ + \mathbf{P}^{\text{T}} \mathbf{C}_{\text{P}}^{-1} P \\ + \mathbf{G}_{\nu}^{\text{T}} \mathbf{C}_{\nu}^{-1} \mathbf{G}_{\nu} \\ + \mathbf{G}_{\phi}^{\text{T}} \mathbf{C}_{\phi}^{-1} \mathbf{G}_{\phi} + \alpha I \end{bmatrix}^{-1} \right. \\ &\left. \times \begin{bmatrix} \mathbf{G}^{\text{T}} \mathbf{C}_{\text{obs}}^{-1} (\mathbf{d}_{\text{obs}} - \boldsymbol{g}(\mathbf{m}_{\text{n}})) \\ + \mathbf{P}^{\text{T}} \mathbf{C}_{\text{P}}^{-1} (\mathbf{m}_{\text{P}} - \mathbf{m}_{\text{n}}) \\ + \mathbf{G}_{\nu}^{\text{T}} \mathbf{C}_{\nu}^{-1} (\boldsymbol{\nu} - \boldsymbol{\nu}(\mathbf{m}_{\text{n}})) \\ + \mathbf{G}_{\phi}^{\text{T}} \mathbf{C}_{\phi}^{-1} (\phi_R(\mathbf{m}_{\text{n}}) - \phi_S(\mathbf{m}_{\text{n}})) \end{bmatrix} \right). \end{aligned} \tag{5}$$

In Equation (5), $\mathbf{G}$ is the sensitivity matrix of the data with respect to the model parameters; the matrix $\mathbf{P}$ contains the partial derivatives of the *a priori* model $\mathbf{m}_{\text{P}}$ with respect to the model $\mathbf{m}$ and hence in our approach it corresponds to the identity matrix whose dimension is equal to the length of the vector $\mathbf{m}$; $\mathbf{G}_\nu$ and $\mathbf{G}_\phi$ are the partial derivatives with respect to the unknown model parameters $\mathbf{m}$ of the Poisson's ratio $\nu$ and of the porosity $\phi$, respectively. The constant parameter $\alpha$ is a damping factor that stabilizes the solution (Levenberg, 1944; Marquardt, 1963). At each iteration $n$, the parameter $\alpha$ is assumed initially equal to the mean value of the diagonal of the product: $\mathbf{G}^{\text{T}} \mathbf{C}_{\text{obs}}^{-1} \mathbf{G}$ normalized for $n$. Then, if the model $\mathbf{m}_{\text{n+1}}$ does not meet any conditions of validity, $\alpha$ is increased until it does. For very high value of $\alpha$, the model $\mathbf{m}_{\text{n+1}}$ converges to $\mathbf{m}_{\text{n}}$ and the inversion stops since no update occurred. The conditions of validity refer to the physics of the problem: all the terms of the model $\mathbf{m}_{\text{n+1}}$ are positive, the Poisson's ratio $\nu(\mathbf{m}_{\text{n+1}})$ ranges between 0.0 and 0.5, and the porosity $\phi_S(\mathbf{m}_{\text{n+1}})$ and $\phi_R(\mathbf{m}_{\text{n+1}})$ are between 0.0 and 1.0. Any further condition related to the specific adopted porosity relationship is explained in the following.

The number of columns of the matrix $\mathbf{G}_\phi$ is equal to the total number of unknown parameters of the problem, while the number of rows depends on the number of layers in which the porosity constraint is applied. The matrix $\mathbf{G}_\phi$ is non-null only for those unknowns involved in the porosity formulations; thus, if this constraint is applied only in the layer $i$, the matrix reduces to a row vector and it is non-null only for $V_{S,i}$, $V_{P,i}$ and $R_i$, as:

$$\boldsymbol{G}_{\phi,i} = \left[ \cdots 0 \cdots \quad \frac{\partial \phi_S(\mathbf{m})}{\partial V_{S,i}} \cdots \frac{\partial \phi_S(\mathbf{m})}{\partial V_{P,i}} \cdots \frac{\partial \phi_R(\mathbf{m})}{\partial R_i} \cdots \right]. \tag{6}$$

The expressions of the partial derivatives depend on the specific formulas adopted for the porosity.

### Petrophysical relationships for porosity coupling in clean sands

The relationships used to constrain porosity to seismic and resistivity parameters ($\phi_S$ and $\phi_R$, respectively) are selected accounting for the expected site conditions. In this study, we assumed a clean saturated sand for both the synthetic and the real-world examples. For the seismic model, we applied the equation proposed by Foti *et al.* (2002) on the basis of Biot's theory (Biot, 1956a, 1956b):

$$\phi_S = \frac{\boldsymbol{\rho}_S - \sqrt{\boldsymbol{\rho}_S^2 - \frac{4(\rho_S - \rho_F) K_F}{V_P^2 - 2\left(\frac{1-\nu_{SK}}{1-2\,\nu_{SK}}\right) V_S^2}}}{2(\boldsymbol{\rho}_S - \boldsymbol{\rho}_F)}, \tag{7}$$

where $\rho_S$ and $\rho_F$ are the densities of the solid particles and of the fluid, respectively; $K_F$ is the bulk modulus of the fluid; $\nu_{SK}$ is the Poisson's ratio of the dry solid skeleton.

This formula is valid under the assumptions of the low-frequency Biot theory (Biot, 1956a): fully saturated

porous medium, undrained condition and perfect fluid (non-dissipative and inviscid fluid). In addition, equation (7) is formulated assuming that the soil grains are incompressible.

Equation (7) is valid if $\phi_S$ ranges between 0.0 and 1.0, hence the following conditions of validity are applied:

$$\rho_S > \rho_F, \tag{8}$$

$$\frac{{V_P}^2}{{V_S}^2} > 2\frac{1-\nu_{SK}}{1-2\nu_{SK}}, \tag{9}$$

$${V_P}^2 - 2\frac{1-\nu_{SK}}{1-2\nu_{SK}}{V_S}^2 > \frac{4\left(\rho_S-\rho_F\right)K_F}{\rho_S^2}. \tag{10}$$

The partial derivatives of Equation (7) with respect to the model parameters $V_S$ and $V_P$, are, respectively:

$$\frac{\partial\phi_S}{\partial V_S} = \frac{4\frac{1-\nu_{SK}}{1-2\nu_{SK}}K_F V_S}{\left(V_P^2 - 2\frac{1-\nu_{SK}}{1-2\nu_{SK}}V_S^2\right)^2\sqrt{\rho_S^2 - \frac{4\left(\rho_S-\rho_F\right)K_F}{V_P^2 - 2\frac{1-\nu_{SK}}{1-2\nu_{SK}}V_S^2}}}, \tag{11}$$

$$\frac{\partial\phi_S}{\partial V_P} = -\frac{2K_F V_P}{\left(V_P^2 - \frac{2\left(1-\nu_{SK}\right)}{1-2\nu_{SK}}V_S^2\right)^2\sqrt{\rho_S^2 - \frac{4\left(\rho_S-\rho_F\right)K_F}{V_P^2 - 2\frac{1-\nu_{SK}}{1-2\nu_{SK}}V_S^2}}}. \tag{12}$$

For the electrical resistivity, we assumed the Archie's formulation for saturated sand (Archie, 1942), according to which the resistivity $R$ of a fully saturated clean porous medium is function of the porosity $\phi_R$ and of the resistivity of the pore fluid ($R_F$) as:

$$R = a\,{\phi_R}^{-m}\,R_F, \tag{13}$$

in which $m$ and $a$ are empirical constants termed as cementation and tortuosity indices, respectively.

In his work, Archie assumed $a$ equal to 1.0 and found that $m$ varies between 1.3 for unconsolidated sand and 2.0 for consolidated sandstones (Archie, 1942). These parameters are usually defined on the basis of *a priori* information. If the electrical resistivity of both the soil mixture and the fluid are known, the porosity can be estimated from Equation (13):

$$\phi_R = \sqrt[m]{a\frac{R_F}{R}}. \tag{14}$$

Such porosity must range between 0.0 and 1.0, this means that all the involved parameters must be real positive values and in addition the following condition of validity must be respected:

$$R > a\ \ R_F. \tag{15}$$

The partial derivative of Equation (14) with respect to the model parameter $R$ is

$$\frac{\partial\phi_R}{\partial R} = -\frac{1}{m\,R}\sqrt[m]{a\frac{R_F}{R}}. \tag{16}$$

To ensure the validity of porosity formulations in Equations (7) and (14), the conditions reported in Equations (8)–(10) and (15) must be respected. Equation (8) on *a priori* parameters is usually implicitly respected since $\rho_S$ is greater than $\rho_F$ for most geomaterials, while the validity conditions in Equations (9), (10) and (15) must be verified at each model update in Equation (5). The partial derivatives (Equations 11, 12 and 16) are then included in the matrix $\mathbf{G}_\phi$ (Equation 6).

In Equations (7) and (14), we assume that the porosity is a function of the model parameters $V_S$, $V_P$ and $R$ of the soil mixture. Thus, all the petrophysical parameters, $\rho_S$, $\rho_F$, $K_F$, $\nu_{SK}$, $a$, $m$ and $R_F$ are assumed *a priori* on the basis of laboratory tests, literature data (some useful suggestions are given by Carmichael (1982), Santamarina (2001) and Friedman (2005)) or other *a priori* information. The petrophysical parameters are assumed constant within each layer. Then, Equations (7) and (14) must be implemented in Equations (5) and (6) using the proper petrophysical parameters for each layer in which the porosity constraint is applied.

The effect of these *a priori* assumptions depends on the sensitivity of the retrieved values of the porosity to the petrophysical parameters in Equations (7) and (14). We hence investigate the sensitivity by considering, for each parameter, a range of values, assumed from the literature (Table 1), which are common for earth materials and fluids. Assuming a saturated porous medium with a porosity equal to 0.4 and the petrophysical parameters equal to the mean values in Table 1, the geophysical parameters $V_S$, $V_P$ and $R$ are estimated as 170 m/s, 1680 m/s and 205 Ωm, respectively. The porosity was then back-computed perturbing each petrophysical parameter at a time and keeping constant the geophysical parameters and the other petrophysical parameters. The percentage error with respect to the true value of porosity was finally calculated and reported in Fig. 1.

The porosity has little sensitivity to the seismic petrophysical parameters reaching a maximum error of 5.3% for $K_F$. On the other hand, the Archie's parameters (*a* and *m)* play a larger role in the estimation of porosity with a maximum variability of 22% for the parameter $m$. Finally, the resistivity of the fluid is the most critical parameter as the corresponding induced variability on the estimated porosity reaches almost 60%. If Equations (7) and (14) are chosen for the estimation of porosity, we suggest performing this kind of sensitivity analysis of

**Table 1** Ranges for petrophysical parameters in Equations (7) and (14) and corresponding mean values that are assumed in the sensitivity analysis

| Parameters | | | Min | Max | Mean | description |
|---|---|---|---|---|---|---|
| **Seismic** | $\rho_S$ | (Kg/m$^3$) | 2550 | 2750 | 2650 | Minerals such as K-feldspar, quartz and calcite (Santamarina, 2001) |
| | $\rho_F$ | (Kg/m$^3$) | 970 | 1030 | 1000 | Fluids such as pure water and seawater (Santamarina, 2001) |
| | $K_F$ | (GPa) | 2.12 | 2.24 | 2.18 | Soils (Santamarina, 2001) |
| | $\nu_{SK}$ | (-) | 0.1 | 0.4 | 0.25 | (Salem, 2000) |
| **Resistivity** | $a$ | (-) | 0.8 | 1.2 | 1 | (Carmichael, 1982) |
| | $m$ | (-) | 1.3 | 2 | 1.65 | (Archie, 1942) |
| | $R_F$ | (Ωm) | 10 | 80 | 45 | Non-contaminated groundwater (Carmichael, 1982) |

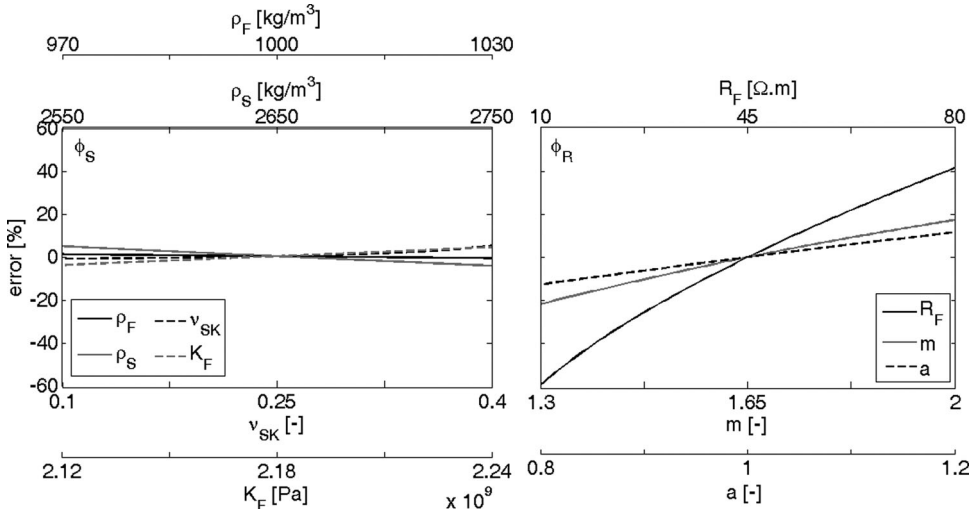


**Figure 1** Sensitivity of porosity to petrophysical parameters in Equations (7) and (14). On the left, porosity estimation from seismic velocities $\phi_S$. The petrophysical parameters are: density of soil grain ($\rho_S$), density of fluid ($\rho_F$), bulk modulus of fluid ($K_F$) and Poisson's ratio of the solid skeleton ($\nu_{SK}$). On the right, porosity estimation from resistivity $\phi_R$. The petrophysical parameters are: resistivity of the fluid ($R_F$), cementation factor ($m$) and tortuosity factor ($a$).

the assumed *a priori* petrophysical parameters with respect to the geophysical ones before the physical joint inversion.

### Synthetic model

We applied the proposed inversion approach to a synthetic example. The porosity constraint is applied to a saturated sand layer by adopting the aforementioned relationships. We then compared the results for different levels of coupling in the inversion to illustrate the advantages of the proposed joint inversion.

### The 1D model and the data

We used a simple one-dimensional synthetic model composed of a sand deposit overlying a half space whose top is placed at 15-m depth. The water table is at 5-m depth, and it is the boundary between the shallow unsaturated sandy layer and the saturated one. We assumed a porosity equal to 0.4 for the sand. Petrophysical parameters were assigned on the basis of literature data (Santamarina, 2001; Comina *et al.*, 2010) and are reported in Table 2. Based on these assumptions, the geophysical model parameters of the sand layer were computed with Equations (7) and (14) and are reported in Table 3. In the same table, the model parameters for the half space are reported. The synthetic data (Fig. 2) were computed using the same forward codes implemented for the inversion algorithm, hence committing an 'inversion crime' since no uncertainty due to the choice of a more suitable forward modelling for the phenomenon was introduced. This strategy is justified by the motivation of this synthetic test, which is comparing the results of the inversion with different level of constraints. We added noise to the synthetic data computed for each sample as

**Table 2** Petrophysical parameters adopted in the synthetic model for the sand deposit and the pore fluid

| Parameters | | Value |
|---|---|---|
| **Seismic** | $\rho_S$ | 2650 Kg/m$^3$ |
| | $\rho_F$ | 1000 Kg/m$^3$ |
| | $K_F$ | 2.18 GPa |
| | $\nu_{SK}$ | 0.227 |
| **Resistivity** | $a$ | 1 |
| | $m$ | 1.8 |
| | $R_F$ | 50 Ωm |

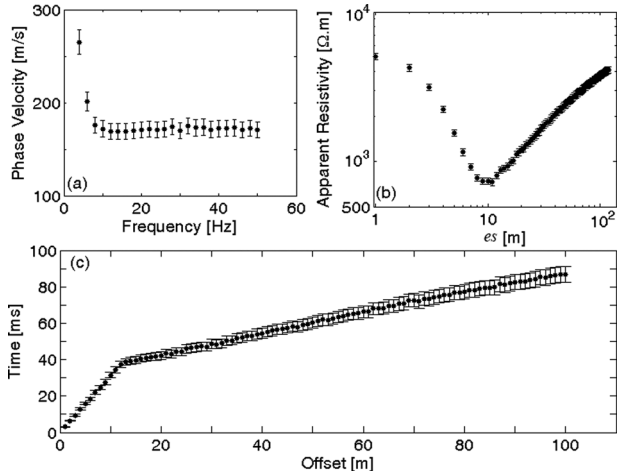


**Figure 2** Synthetic data: (a) dispersion curve **dc**, (b) apparent resistivity curve **ar** and (c) P-wave traveltime **pwt**.

a random percentage between −2.5% and 2.5% of the value of the sample itself. As far as the standard deviation is concerned, in any experimental data set, it can be related to the sampling interval adopted for the measurement, or to a statistical analysis if the measurement is repeated a significant number of times or any other kind of source of this information. However, in the proposed synthetic case, we assumed a reliable value for the standard deviation equal to 5% of the simulated data.

### Effect of porosity constraint on the solution space

Before showing the inversion results, we here evaluate how the porosity constraint would potentially reduce the non-uniqueness of the solution for the considered model and data. We computed the value of the objective function (Equation 4) in the absence of porosity constraint (only the first three terms of Equation 4) and with the addition of the constraint of porosity (all four terms in Equation 4) applied to the saturated sand layer only (layer n. 2 in Table 3). The misfit was computed with a grid of step 0.8 m/s for $V_S$, 8.0 m/s for $V_P$ and 0.3 Ωm for $R$, varying in a range ±20% of their values in the saturated sand layer (Table 3), while all the other model parameters are assumed as the true ones. We show the results in Fig. 3 in the three different domains: $V_P$-$V_S$; $V_P$-$R$; and $V_S$-$R$. In each domain, the third parameter is kept equal to the true value.

The misfit surface without porosity constraint (Fig. 3, left panels) has a flatter shape than that obtained by introducing the constraint on porosity (Fig. 3, right panels). In particular, the porosity constraint affects the misfit associated to $V_P$ and $R$ as they are strongly affected by the pore fluid, while $V_S$ is only slightly influenced by it.

### Initial model and inversion results

As a local search approach is implemented in the inversion code, an accurate selection of the initial model is of paramount importance. The number of layers of the model was assumed equal to the true model itself, and hence two layers over a half space to focus more on the improvements of the physical constraints while the initial model parameter values were estimated from a preliminary interpretation of the data to be inverted as suggested in Piatti *et al.* (2013) and Boiero and Socco (2014). Furthermore, since a physical joint inversion is applied, also the initial model parameters must respect all the conditions of validity (Equations 8, 9, 10 and 15). The initial model parameters are summarized in Table 4, while the initial model parameters and the forward responses of the initial model are shown in Figs. 4 and 5, respectively. Since $V_P$ and $V_S$ initial models were conceived independently, the implied Poisson's ratio can be calculated (Table 4). It is quite close to the true value in the saturated layer and in the bedrock, but not in the first layer.

Since the formulation of the seismic porosity (Equation 7) is valid only for saturated conditions, the porosity constraint is applied only to the model parameters of the second layer, where a saturated porous medium is simulated.

The petrophysical parameters are assumed equal to the true ones (Table 2) in order to verify if the inversion algorithm properly solves the model. Moreover, the *a priori* model $\mathbf{m_P}$ was assumed equal to the initial one (Table 4) with a very weak constraints implemented in the matrix $\mathbf{C_P}$ (the terms along the diagonal are equal to $10^6$). As far as the expected values of the Poisson's ratio $\nu$ are concerned, these were assumed equal to the ones computed from the *a priori* model (Table 4) with a very week constraint (all the terms along the diagonal of

**Table 3** Geophysical model parameters of the synthetic model

| Layer | h (m) | $\rho$ (kg/m$^3$) | $\nu$ (-) | $V_S$ (m/s) | $V_P$ (m/s) | $R$ (m) |
|---|---|---|---|---|---|---|
| **1- unsaturated sand** | 5 | 1590 | 0.227 | 190 | 320 | 5200 |
| **2- saturated sand** | 10 | 1990 | 0.495 | 170 | 1680 | 260 |
| **3- half space** | – | 2400 | 0.485 | 350 | 2000 | 7000 |

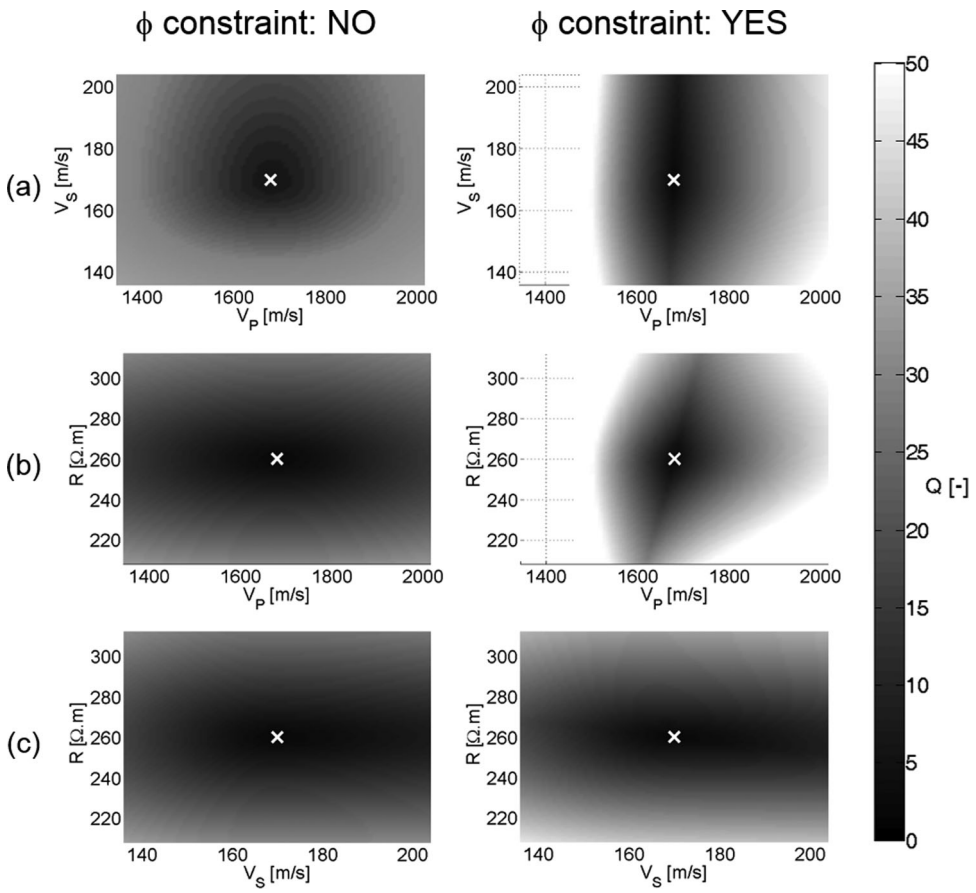


**Figure 3** Misfit function computed according to Equation (5) without (left) and with (right) the contribution of the porosity constraint in a range of 170 ± 20% for $V_S$, 1680 ± 20% for $V_P$ and 260 ± 20% for $R$. The misfit function is reported in three different domains: (a) $V_P$-$V_S$; (b) $V_P$-$R$ and (c) $V_S$-$R$. The white cross represents the true model.

**Table 4** Model parameters of the initial and *a priori* models of synthetic data inversion

| Layer | h (m) | $\rho$ (kg/m$^3$) | $\nu$ (-) | $V_S$ (m/s) | $V_P$ (m/s) | R (Ωm) |
|---|---|---|---|---|---|---|
| **1** | 3 | 1700 | 0.405 | 200 | 500 | 5000 |
| **2** | 3 | 1900 | 0.486 | 300 | 1800 | 700 |
| **Half space** | – | 2200 | 0.474 | 400 | 1800 | 3000 |

the matrix $\mathbf{C}\nu$ are equal to 1.0). Moreover, it ensures that the Poisson's ratio does not assume values outside the physical range from 0.0 to 0.5 by imposing a validity condition through the damping term $\alpha$.

Several inversions were performed: (i) *individual* inversions: each data set is inverted independently from the others; (ii) *structural* inversion: all the data sets are inverted simultaneously without applying any physical constraint but

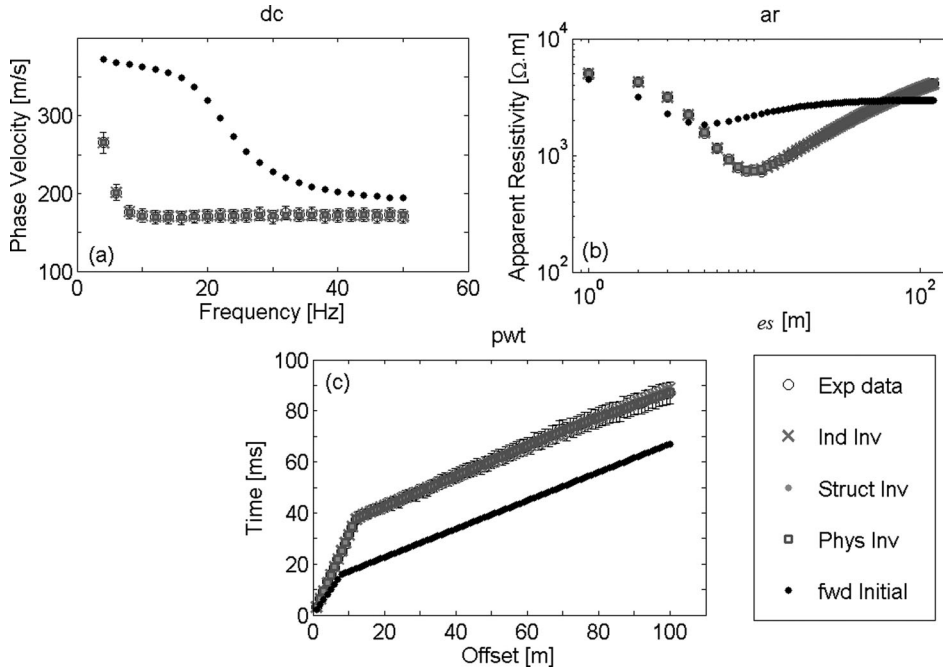


**Figure 4** Fitting between the data and the forward response of the final model resulting from different inversions: (a) dispersion curve, (b) apparent resistivity and (c) P-wave traveltimes.

assuming a shared one-dimensional geometry for the different models; and (iii) *physical* inversion: all the data are inverted applying the Poisson's ratio and porosity as physical constraints among the model parameters, in addition to the structural constraint.

Figure 4 shows the data sets compared to the forward responses for the final models of each inversion. The results are reported in Fig. 5.

Although all the forward responses fit well the data (Fig. 4), the $V_S$ and $V_P$ profiles (Fig. 5a and b, respectively) resulting from the *individual* inversion are quite far from the true ones, and this leads to an estimation of the Poisson's ratio (Fig. 5d) which is close to zero in the unsaturated layer. On the contrary, the resistivity model is solved quite well (Fig. 5c) with the *individual* inversion. Moreover, the interfaces in these final models are not consistent with each other. The *structural* inversion provides a significant improvement with final models that are in good agreement with the true ones and all of them identify common interfaces. Finally, when the physical constraints are applied, the final model is further improved and the interface between the second layer and the half space is better resolved as well as the Poisson's ratio profile.

The error between the estimated model parameters and the true ones is reported in Fig. 6. The error on the thicknesses is quite high in the dc and pwt *individual* inversions, reaching almost 100%. The errors for all model parameters are reduced to less than 10% when the *structural* joint inversion is applied, and the maximum error further decreases to less than 3.5% with the *physical* joint inversion.

The porosity was computed from S- and P- wave velocities ($\phi_S$, Equation 7) as well as from resistivity ($\phi_R$, Equation 14) in the second layer for all the computed models (Fig. 7). Since the individual inversion provides $V_S$ and $V_P$ models whose interfaces are not consistent with each other, the porosity profile varies with depth within the saturated layer (5–15 m depth). Between 4.5 m and 7.5 m depth, $V_P$ is equal to 1120 m/s, a value that is not consistent with a saturated sand. Thus, the condition of saturation is not respected for Equation (7) and the porosity assumes a not realistic value (Not a Number, NaN). In the *structural* inversion, the porosity was equal to 0.38 and 0.42 from seismic and resistivity, respectively, while in the physical inversion the two quantities converge on 0.395, quite close to the true value (0.4).

Despite all the final models provide a good fitting with the data (Fig. 4), the one resulting from the joint physical inversion is the better resolved. Moreover, the porosity values from seismic and resistivity parameters converge on the same value, which is very close to the true one.

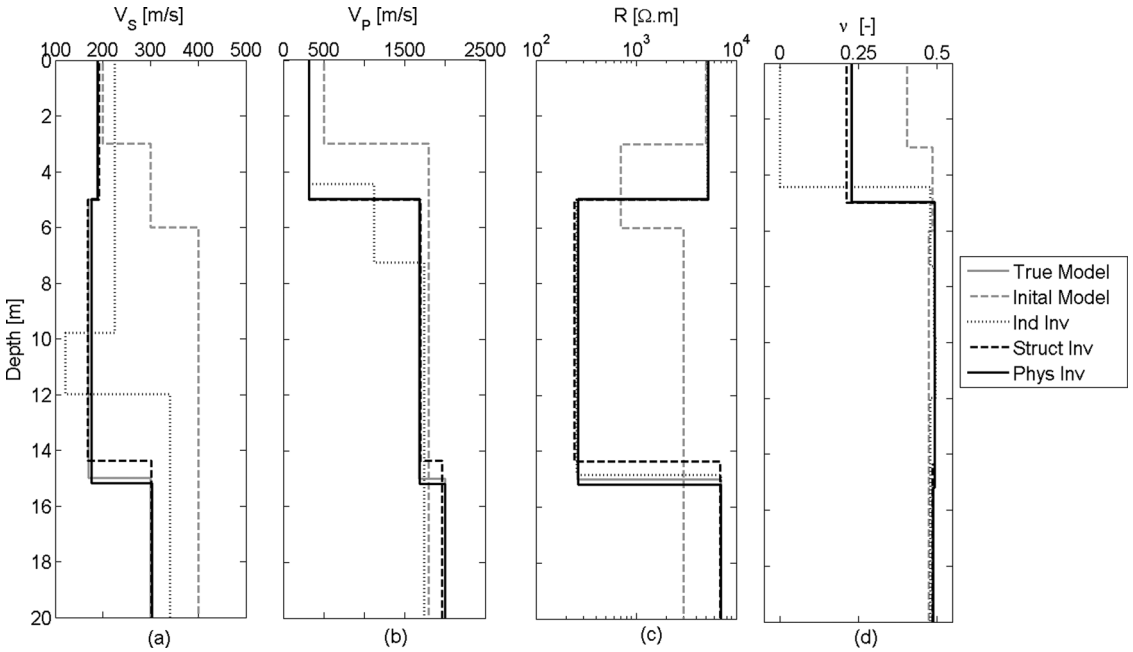


**Figure 5** Initial models (grey dashed line) and final models resulting from individual inversion (black dotted line), structural inversion (black dashed line), and physical inversion (black solid line) compared with the true one (grey solid line): (a) S-wave velocity, (b) P-wave velocity, (c) Resistivity and (d) Poisson's ratio resulting from $V_P$ and $V_S$ profiles.

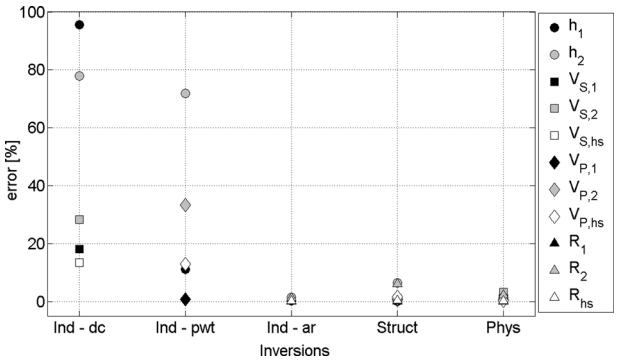


**Figure 6** Error between the estimated model parameters and the true ones, for the individual, structural and physical inversions.

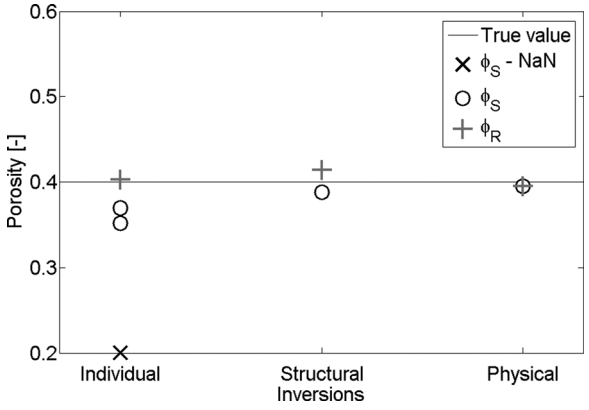


**Figure 7** Porosity estimation from seismic velocities ($\phi_S$) and resistivity ($\phi_R$) models for the different inversions. These values are estimated in the portion of the model where the saturated sand is expected.

## CASE STUDY

### Site description and experimental data

The site is located in the floodplain zone, the area between the river and the embankment, in the Padana plain, Northern Italy (Fig. 8). In 2001, Comina *et al.* (2004) carried out a geophysical campaign with both seismic and electrical methods applied along several profiles in and out the Po River embankment aimed at investigating the foundation soil. The subsurface is a stack of soil layers with a clayey layer embedded between sandy layers as suggested by Colombo (1964, Fig. 9) and the water table in the shallow sandy layer is expected to vary between 4-m and 5-m depth in the area close to the Po River where the presented data were acquired.

The data used in this work are from a profile located between the river and the embankment (Fig. 8, right) where the top layer is constituted of loose sand deposited by the Po River. Along the profile, Comina *et al.* (2004) acquired for their study seismic data for P-wave seismic refraction tomography but in our case we just used the end-on shot (the shot at

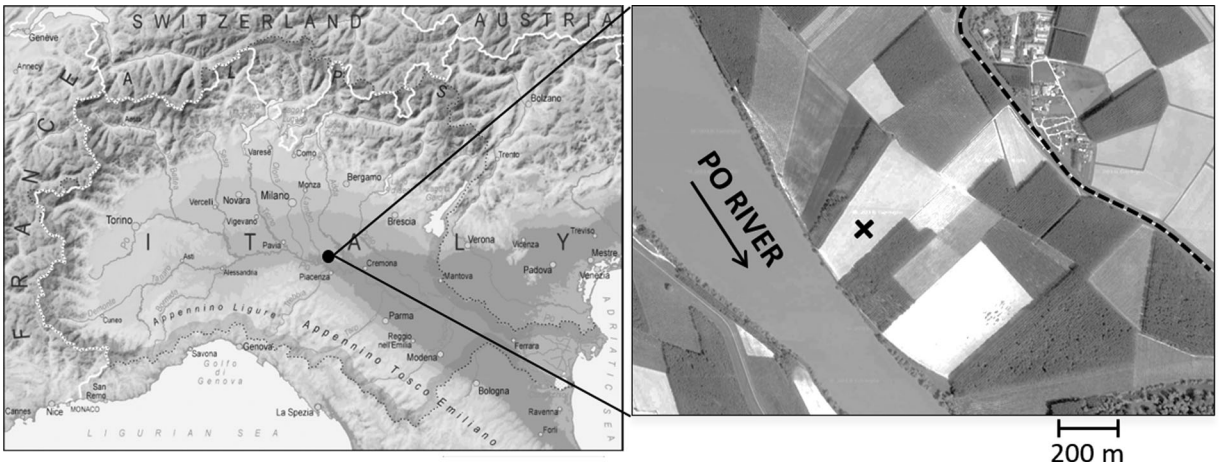


**Figure 8** On the left, location of the site in the Po River basin, Northern Italy. On the right, location of the survey (black cross) between the river and the embankment (dashed line).

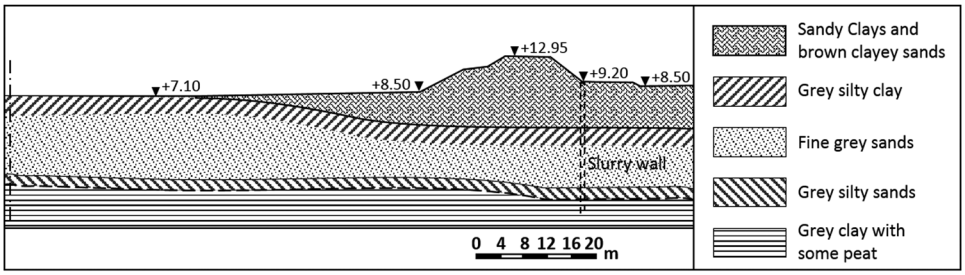


**Figure 9** Example of the section of the foundation soil of the embankment on the left Po River bank (after Colombo, 1964).

**Table 5** Acquisition parameters for Surface wave method and P-wave refraction surveys

| Parameter | Surface Wave | P-wave refraction |
|---|---|---|
| Array length (m) | 24 | 72 |
| Receiver spacing (m) | 1 | 3 |
| Recording Length (ms) | 4096 | 102.4 |
| Sampling rate (ms) | 2 | 0.05 |
| Number of shots | 1 | 1 |
| Source | Sledge hammer (6 Kg) | Sledge hammer (6 Kg) |

the beginning of the line) for our one-dimensional study. In addition to this, data for surface wave method and vertical electrical sounding were also available. The acquisition parameters for the seismic methods are reported in Table 5 while the apparent resistivity data were acquired using a Schlumberger configuration and maximum electrode spacing is equal to 70 m.

Figures 10(a) and 11 show the seismograms of Surface wave and P-wave refraction surveys, respectively. Figure 10(b) shows the frequency-wave number spectrum with the picked dispersion curve. The data (dispersion curve, P-wave traveltimes and apparent resistivity curve) are reported in Fig. 12.

### Definition of the initial and *a priori* models and inversion results

The *a priori* reference model ($\mathbf{m_P}$ in Equation 4) was defined on the basis of previous studies performed in the area (Comina *et al.*, 2004) and a preliminary interpretation of the data. Furthermore, these sources of information support the absence of lateral variations in the site and hence they make reliable the choice of the one-dimensional model. The *a priori* reference model is summarized in Table 6. The intercept time method applied to the P-wave traveltime curve (Fig. 12b) provided a shallow layer 4.5 m thick with $V_P$ equal to 250 m/s overly-

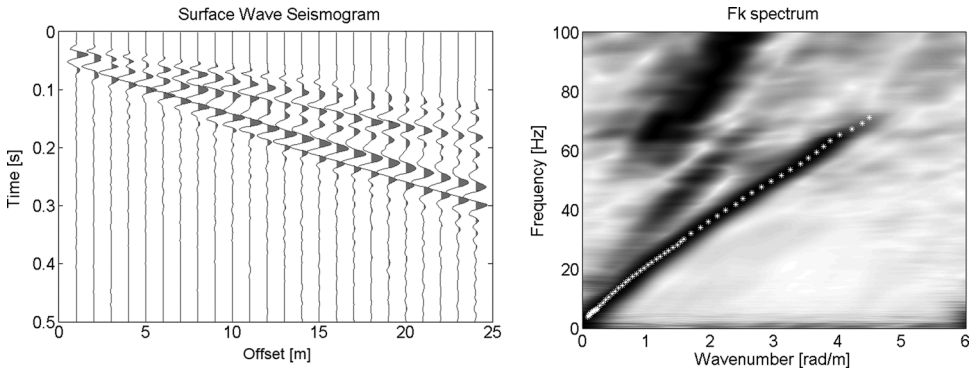


**Figure 10** Surface Wave survey: on the left the raw data and on the right the related frequency-wavenumber (f-k) spectrum in which the dispersion curve is picked (white stars).

**Table 6** *A priori* and initial models for the field case. It is defined in terms of depth, thickness of the layer ($h$), density ($\rho$), Poisson's ratio ($\nu$), S-wave velocity ($V_S$), P-wave velocity ($V_P$) and resistivity ($R$)

| Layer | Depth (m) | h (m) | $\rho$ (kg/m3) | $\nu$ (-) | $V_S$ (m/s) | $V_P$ (m/s) | R (Ωm) |
|---|---|---|---|---|---|---|---|
| **1** | 0.5 | 0.5 | 1550 | 0.23 | 100 | 170 | 190 |
| **2** | 1.25 | 0.75 | 1550 | 0.25 | 110 | 190 | 200 |
| **3** | 2.5 | 1.25 | 1600 | 0.27 | 140 | 250 | 210 |
| **4** | 4.5 | 2 | 1600 | 0.26 | 170 | 300 | 250 |
| **5** | 7 | 2.5 | 1700 | 0.49 | 230 | 1800 | 100 |
| **6** | 12 | 5 | 1800 | 0.49 | 200 | 1800 | 70 |
| **Half space** | – | – | 1800 | 0.49 | 300 | 1800 | 100 |

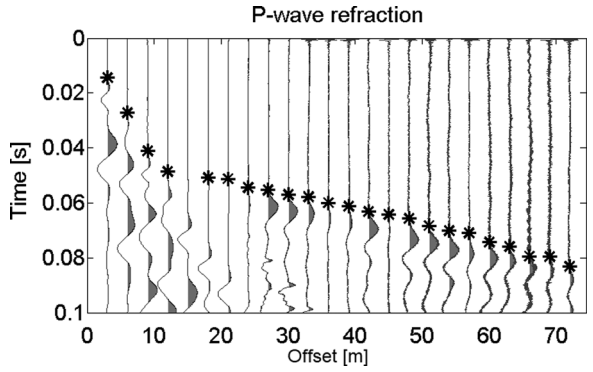


**Figure 11** P-wave refraction survey: seismogram for the shot in $x =$ 0 m. The black stars are the picked P-wave traveltimes.

ing an 1800 m/s half space. The shallow layer, attributed to unsaturated sand, was further divided in four sub-layers with seismic velocity profiles increasing with depth according to a power-law trend typical of unconsolidated dry granular materials (Gassmann, 1951; Bachrach et al., 1998, 2000). For this shallow zone, the $V_S$ values were chosen according to reasonable values of Poisson's ratio for unsaturated sand (Santamarina, 2001), while the $R$ profile was assumed to increase with depth from 190 Ωm to 250 Ωm according to the available experimental data for apparent resistivity (Fig. 12c). Below 4.5 m depth, a saturated sand with a clay lens is expected, hence two layers over a half space were added. In these two layers, saturated sand and clay, and in the half space, the $V_P$ was assumed homogeneously equal to 1800 m/s since the P-wave traveltime curve (Fig. 12b) shows a very smooth behaviour for offset greater than the crossover point at around 12 m and 1800 m/s, which is the value that, in a first instance, describes this trend. Since the trend of the apparent resistivity shows a minimum for *es* roughly around 35 m (Fig. 12c), a decrease in the $R$ profile is expected and hence the initial model was assumed equal to 70 Ωm in the layer between two layers with resistivity equal to 100 Ωm. Since the low resistivity layer is likely associated to a clay layer, we also expected a decrease of $V_S$ as confirmed by a previous study (Comina, *et al.*, 2004). The density was assumed to increase with depth from 1550 Kg/m$^3$ to 1800 Kg/m$^3$, a typical range for soil mixtures (Santamarina, 2001). As for the synthetic case, this model (Table 6) respects the conditions of validity (Equations 8, 9, 10 and 15).

The covariance matrix $\mathbf{C_P}$ associated to the *a priori* model $\mathbf{m_P}$ was set to have weak constraints ($10^6$ in the diagonal of the matrix). The expected value of the Poisson's ratio $\nu$ was computed from the *a priori* model $\mathbf{m_P}$ and weak constraint

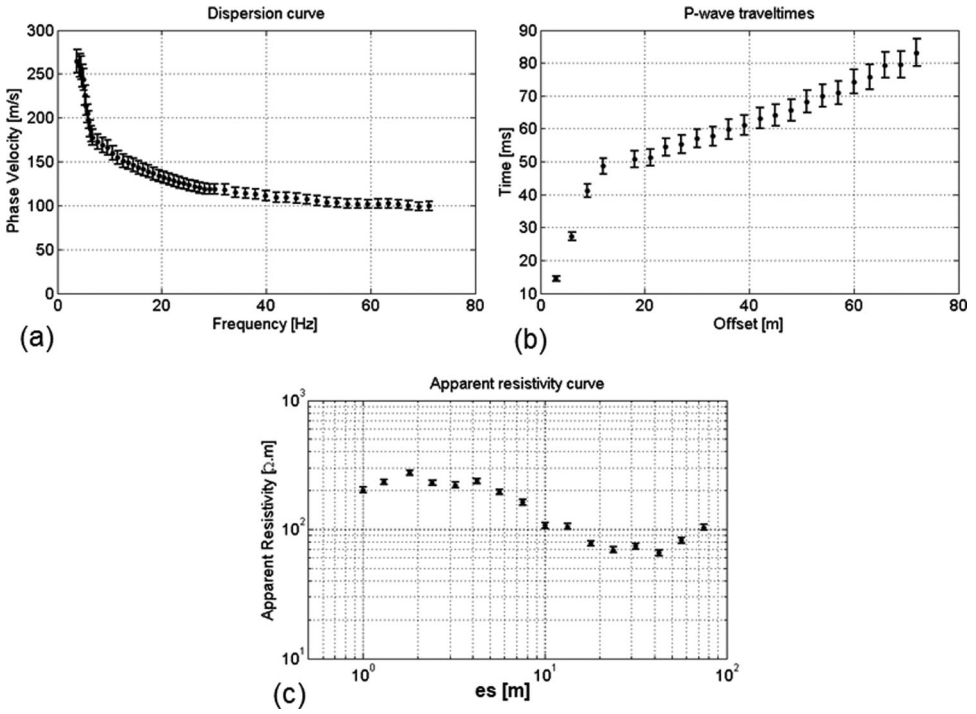


**Figure 12** Field data: (a) dispersion curve, (b) P-wave traveltimes and (c) apparent resistivity curve.

**Table 7** Petrophysical parameters assumed for the porosity estimation in the saturated sandy layer

| Parameters | | Value |
|---|---|---|
| **Seismic** | $\rho_S$ | 2650 Kg/m$^3$ |
| | $\rho_F$ | 1000 Kg/m$^3$ |
| | $K_F$ | 2.18 GPa |
| | $n_{SK}$ | 0.227 |
| | *Initial* $\phi_{S,5}$ | 0.33 |
| **Resistivity** | $a$ | 1 |
| | $m$ | 1.3 |
| | $R_F$ | 30 Ωm |
| | *Initial* $\phi_{R,5}$ | 0.38 |

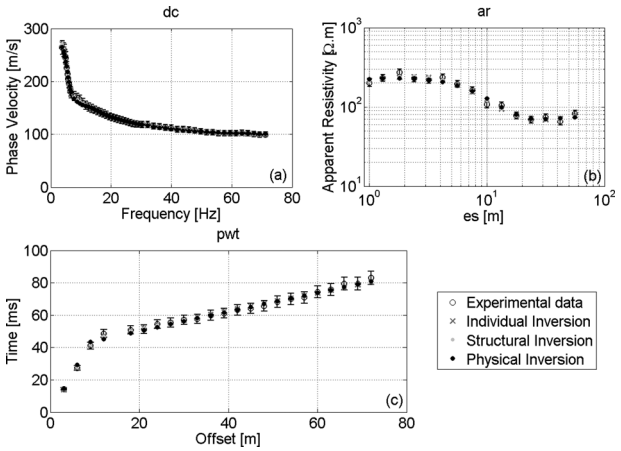


**Figure 13** Fitting between the experimental data and the forward response of the final models: (a) dispersion curve, (b) apparent resistivity and (c) P-wave traveltimes.

were associated (1 in the diagonal of the matrix $\mathbf{C}_v$). The initial model **m** was set equal to the *a priori* one (Table 6). The porosity constraint was applied to layer 5, where the saturated sand is expected. The petrophysical parameters for the computation of seismic porosity (Equation 7) were assumed equal to the ones used for the synthetic case (Table 2). The petrophysical parameters used in Equation (14) for the computation of porosity from resistivity data were assumed according to Carmichael (1982) and to previous studies in the area (Comina *et al*., 2004). All the assumed petrophysical parameters are reported in Table 7 as well as the initial porosity in the expected saturated sandy layer (layer 5 in Table 6) that is equal to 0.33 and 0.38 from seismic velocities and resistivity, respectively.

Different inversions were run: (i) *Individual inversion*; (ii) *Structural joint inversion*; (iii) *Physical joint inversion*.

The forward responses of the final models for all the inversions honour quite well the data (Fig. 13) even if for **pwt**

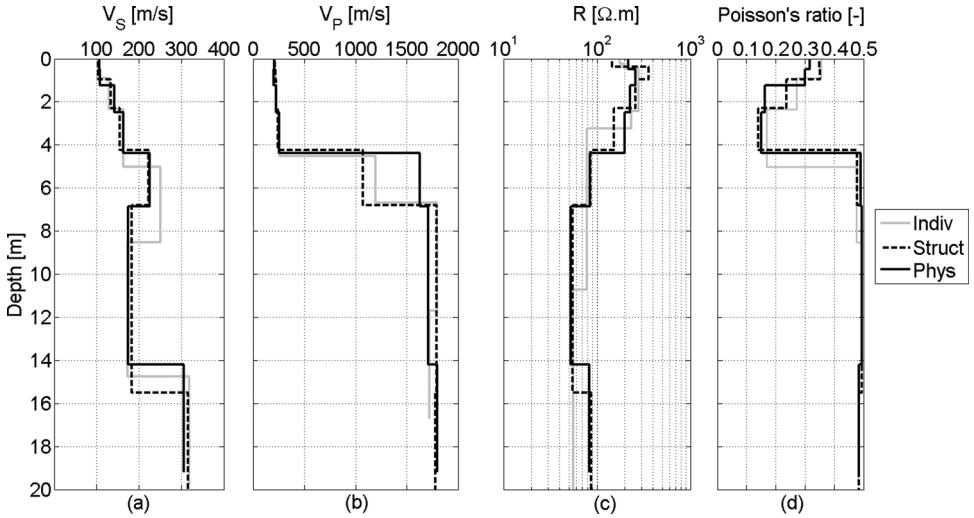


**Figure 14** Final models obtained performing different inversions: *individual*, *structural*, *Physical*. In (a) S-wave velocity, in (b) P-wave velocity, in (c) Resistivity and in (d) the Poisson's ratio.

and **ar** some data points calculated for the final model of both structural and physical joint inversions are at the edge of the uncertainty bar. Figure 14 shows the final model for each inversion. The interfaces of the profiles from individual inversions are not consistent with each other, but this consistency is imposed with the joint inversions. In addition, the profiles are further adjusted by applying the physical constraints. The physical constraints improve the $V_P$ estimation in the expected saturated sand layer at around 4–5 m (Fig. 14b), reaching values that are more consistent with the theoretical expected values in such materials. Indeed the value of $V_P$ in the range 1000–1200 m/s (as obtained without imposing the physical constraints, Fig. 14b) not only are not consistent with the other study performed in the surrounding of the site (Comina *et al.*, 2004), but also it is not consistent with Biot theory for wave propagation in saturated porous media (Biot, 1956b). As far as the water table is concerned, this is expected at 4–5 m, but in the resistivity profile from individual inversion, the decrease in resistivity is located at 3.2 m, while $V_P$ shows values which are not in agreement with saturated sand and hence the water table cannot be identified at all. Due to all the synergies in the physical joint inversion, the water table is uniquely identified at 4.3 m.

Figure 15 reports the values of porosity in the saturated sandy layer as estimated from the final models of Fig. 14. Despite the initial geophysical parameters were chosen such that the porosity estimations at layer 5 were reliable, even if not convergent, the individual and structural inversions provided values of $V_P$ that lead to an error in the evaluation of soil porosity with Equation (7) (as the quantity under square root

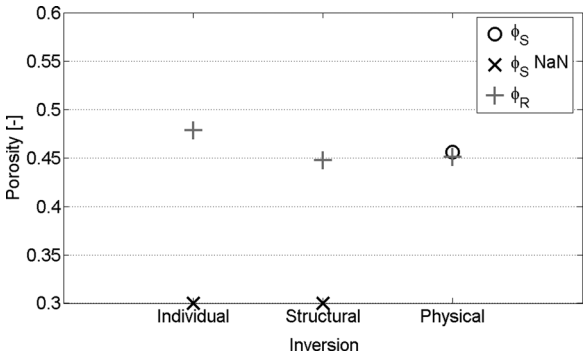


**Figure 15** Porosity estimations from resistivity and seismic velocities in the saturated layer. NaN stands for 'Not-a-Number', that is, the value cannot be calculated.

becomes negative). The porosity values estimated using seismic and resistivity converge to 0.45 when the physical constraints are applied. This value is in good agreement with Bellotti and Selleri (1969), who performed a geotechnical characterization of the alluvial sediments in several locations in the Padana plain deducing a range for the porosity between 0.42 and 0.52.

Although the porosity constraint is applied to the saturated layer only and the Poisson's ratio is applied only to constraint $V_P$ and $V_S$ to the acceptable physical range 0.0–0.5, these help to improve the whole final model. For example, the $V_S$ and $V_P$ profiles, obtained when the physical constraints are applied, provide in the shallow unsaturated layer a Poisson's ratio equal to 0.13 (Fig. 14d) that is in good agreement with the one estimated by Bergamo and Socco (2016) through a

multimodal inversion of the dispersion curve. Only in the very shallow part of the model, less than 1-m deep, the Poisson's ratio is not consistent with that result: in this small range, the $V_P$ is not well resolved since a receiver spacing equal to 3 m is adopted in the P-wave refraction survey.

## DISCUSSION

The proposed algorithm performs a one-dimensional (1D) joint inversion of surface-wave dispersion, P-wave traveltimes and apparent resistivity data from vertical electrical sounding adopting both structural and physical constraints and is applied to the characterization of soil deposits containing a saturated sand layer. In addition to the Poisson's ratio, that links P-wave and S-wave velocities to each other, the algorithm was further developed by introducing a constraint between the seismic velocities and the resistivity through the porosity. The constraint of porosity among seismic velocities and electrical resistivity requires the choice of appropriate petrophysical relationships for the expected materials. In the present work, an example based on two widely used formulations (Equations 7 and 14) for clean saturated sands is reported. In these formulations, some petrophysical parameters are defined *a priori* in the inversion process. Among these parameters, the most critical is the resistivity of the pore fluid (Fig. 1) while for the others, especially the parameters in the seismic formulation of porosity, the sensitivity of the porosity to their values is low. Review of previous studies or information from borehole logs can be used to define reliable values of the petrophysical parameters. However, we suggest performing a sensitivity analysis on the *a priori* petrophysical parameters with respect to the geophysical ones before running the physical joint inversion to better investigate the impact of the assumed *a priori* parameters.

The synthetic example provides a benchmark for the proposed approach. The inclusion of the porosity constraint is shown to reduce the non-uniqueness of the solution (Fig. 3) and the physical joint inversion leads to an internally consistent final model. The joint physical inversion provides a final model whose estimation of porosity and Poisson's ratio are very close to the true values. Other inversions provide final models that are not internally consistent for the computation of porosity (Fig. 7). As for the error between the calculated and the true model parameters, it reduces considerably when the structural constraint is included in the joint inversion. The physical constraints provided by Poisson's ratio and porosity lead to a further improvement in the estimation (Fig. 6).

In the field case, even if the misfit between the forward response and the data of both structural and physical joint inversions is slightly higher than the individual inversions, the final model obtained with both Poisson's ratio and porosity constraints is more reliable and allows for a consistent estimation of soil porosity, and the obtained value is in agreement with other studies (Bellotti & Selleri, 1969). The Poisson's ratio constrains the estimation of model parameters in the acceptable domain for the elastic theory and hence the porosity constraint can be applied leading to a final model that is physically reliable. The individual inversions may provide a good fitting and a very low misfit but this may be due to an overfit of the noise in the data, or because they converge towards models that are not physically consistent but still within the range associated to solution non uniqueness. On the other hand, the joint inversion imposes a compromise among the results of different methods that have different resolutions. Therefore, it may result in a slight increase of the misfit, particularly in case of noisy data, but the final model is physically consistent and honours the whole experimental data set.

The approach here proposed requires a good *a priori* knowledge of the site for the choice of the proper physical relationship and the layer where it should be applied. This approach could be adopted as refinement of P- and S- wave velocities and resistivity models to obtain final models which are physically consistent with each other.

The present work is limited to a 1D model with the only focus on the introduction of the physical relationship to constraint the geophysical model parameters in the joint inversion. Once assessed, this application could be straightforwardly extended to especially to all those joint inversion scheme of P-wave refraction, surface-wave dispersion and apparent resistivity data, based on several local 1D models that are spatially constrained to build pseudo two-dimensional (2D) or pseudo three-dimensional (3D) models (e.g., Garofalo *et al.*, 2015).

As far as the computational cost is concerned, it is not a critical issue in this case of a 1D layered model with few unknowns (11 and 27 for the synthetic and real case studies, respectively) and we did not observe significant difference in the overall computational time between running the three individual inversions and one joint inversion. In a 2D or 3D model, most of the computational cost is due to the chosen forward response and to the Jacoban matrix obtained often as forward modelling of perturbated model parameters. The physical constraint, as presented here, is only an equation among some of the total amount of unknowns and hence its impact should be negligible on the overall computational time.

## CONCLUSION

We presented an algorithm for the joint inversion of surface-wave, P-wave traveltimes and apparent resistivity data from vertical electrical sounding. Poisson's ratio and porosity are adopted as physical relationships to constrain the inversion and reduce the non-uniqueness of the solution. We used porosity equations valid for clean saturated sand, but the joint inversion scheme can be extended using appropriate formulation of porosity for the investigated medium.

Even if the Poisson's ratio and the porosity are not primary objectives of the inversion, the final geophysical model is solved by imposing them as constraints. The final model is then physically consistent and provides a reasonable estimation of Poisson's ratio and porosity and hence these can be considered as relevant side products.

The parameterization is based on a 1D model obtaining promising results for an application on a 2D or 3D models.

The data that support the findings of this study are available from the corresponding author on reasonable request.

## ACKNOWLEDGEMENTS

The authors would like to thank Cesare Comina and Luigi Sambuelli for sharing with us the field data that they acquired in the Padana plain and here presented in the case study.

## ORCID

*Flora Garofalo* https://orcid.org/0000-0002-4791-8148
*Laura Valentina Socco*
https://orcid.org/0000-0001-8830-9050
*Sebastiano Foti* https://orcid.org/0000-0003-4505-5091

## REFERENCES

Archie, G.E. (1942) The electrical resistivity log as an aid in determining some reservoir characteristics. *Transactions of the American Institute of Mining, Metallurgical and Petroleum Engineers*, 146, 54–62.

Aster, R.A., Brochers, B. & Thurber, C.H. (2005) *Parameter estimation and inverse problems*. 1, Cambridge: Elsevier Academic Press.

Auken, E. & Christiansen, A.V. (2004) Layered and laterally constrained 2D inversion of resistivity data. *Geophysics*, 69(3), 752–761. https://doi.org/10.1190/1.1759461

Bachrach, R., Dvorkin, J. & Nur, A. (1998) High-resolution shallow-seismic experiments in sand, Part II: Velocities in shallow unconsolidated sand. *Geophysics*, 63(4), 1234–1240. https://doi.org/10.1190/1.1444424

Bachrach, R., Dvorkin, J. & Nur, A.M. (2000) Seismic velocities and Poisson's ratio of shallow unconsolidated sands. *Geophysics*, 65(2), 559–564. https://doi.org/10.1190/1.1444751

Backus, G. & Gilbert, F. (1970) Uniqueness in the inversion of inaccurate gross Earth data. *Philosophical Transactions of the Royal Society*, 266, 123–192. https://doi.org/10.1098/rsta.1970.0005

Bergamo, P. & Socco, L.V. (2016) P- and S-wave velocity models of shallow dry sand formations from surface wave multimodal inversion. *Geophysics*, 81(4), R197–R209. https://doi.org/10.1190/geo2015-0542.1

Bellotti, R. & Selleri, G. (1969) Correlazione tra le caratteristiche geotecniche di alcuni terreni di fondazione e confronto tra i risultati ottenibili con l'applicazione di diversi metodi di calcolo del carico ammissibile. *Rivista Italiana di Geotecnica*, 2, 95–103.

Berryman, J.G., Berge, P.A. & Bonner, B.P. (2002) Estimating rock properties and fluid saturation using only seismic velocities. *Geophysics*, 67(2), 391–404. https://doi.org/10.1190/1.1468599

Biot, M.A. (1956a) Theory of propagation of elastic waves in a fluid-saturated porous solid. I. Low-frequency range. *Journal of the Acoustical Society of America*, 28(2), 168–178.

Biot, M.A. (1956b) Theory of propagation of elastic waves in a fluid-saturated porous solid. II. Higher frequency range. *Journal of the Acoustical Society of America*, 28(2), 179–191.

Boiero, D. & Socco, L.V. (2014) Joint Inversion of Rayleigh-wave dispersion and P-wave refraction data for laterally varying layered models. *Geophysics*, 79(4), EN49–EN59. https://doi.org/10.1190/geo2013-0212.1

Bruggeman, D.A.G. (1935) Berechnung verschiederner physikalischer konstanten von heterogenen substanzen. *Annalen Der Physik*, 24, 636–679.

Bussian, A.E. (1983) Electrical conductance in a porous medium. *Geophysics*, 48(9), 1258–1268. https://doi.org/10.1190/1.1441549

Carmichael, R.S. (1982) *Handbook of physical properties of rock*. Boca Raton, FL: CRC Press.

Colombo, P. (1964) *Studio delle caratteristiche dell'argilla limosa degli argini del Po: Istituto di costruzioni marittime*. Università di Padova.

Colombo, D. & Rovetta, D., (2018) Coupling strategies in multiparameter geophysical joint inversion. *Geophysical Journal International*, 215(2), 1171–1184. https://doi.org/10.1093/gji/ggy341

Comina, C., Foti, S., Socco, L.V. & Strobbia, C. (2004) Geophysical characterization for seepage potential assessment along the embankments of the Po River. *Proceedings ISC-2 on Geotechnical and Geophysical Site Characterization*, 451–458. http://hdl.handle.net/2318/58979

Comina, C., Cosentini, R.M., Foti, S. & Musso, G. (2010) Electrical Tomography as laboratory monitoring tool. *Rivista Italiana di Geotecnica*, 44, 15–26.

Dal Moro, G. (2008) VS and VP vertical profiling via joint inversion of Rayleigh waves and refraction travel times by means of bi-objective evolutionary algorithm. *Journal of Applied Geophysics*, 66, 15–24. https://doi.org/10.1016/j.jappgeo.2008.08.002

de Nardis, R., Cardarelli, E. & Dobroka, M. (2005) Quasi-2D hybrid joint inversion of seismic and geoelectric data. *Geophysical Prospecting*, 53, 705–716. https://doi.org/10.1111/j.1365-2478.2005.00497.x

de Lima, O.A.L. (1995) Water saturation and permeability from resistivity, dielectric, and porosity logs. *Geophysics*, 60(6), 1756–1764. https://doi.org/10.1190/1.1443909

Dell'Aversana, P., Bernasconi, G., Miotti, F. & Rovetta, D. (2011) Joint inversion of rock properties from sonic, resistivity and density well-log measurements. *Geophysical Prospecting*, 59, 1144–1154. https://doi.org/10.1111/j.1365-2478.2011.00996.x

Dobróka, M., Gyulai, Á., Ormos, T., Csókás, J. & Dresen, L. (1991) Joint inversion of seismic and geoelectric data recorded in an underground coal mine. *Geophysical Prospecting*, 39(5), 643–665. https://doi.org/10.1111/j.1365-2478.1991.tb00334.x

Doetsch, J., Linde, N. & Binley, A. (2010) Structural joint inversion of time-lapse crosshole ERT and GPR traveltime data. *Geophysical Research Letters*, 37, L24404. https://doi.org/10.1029/2010GL045482

Domenico, S.N. (1984) Rock lithology and porosity determination from shear and compressional wave velocity. *Geophysics*, 49(8), 1188–1195. https://doi.org/10.1190/1.1441748

Eberhart-Phillips, D., Han, D.-H. & Zoback, M.D. (1989) Empirical relationships among seismic velocity, effective pressure, porosity and clay content in sandstone. *Geophysics*, 54(1), 82–89. https://doi.org/10.1190/1.1442580

Feng, X., Ren, Q., Liu, C. & Zhang, X. (2017) Joint acoustic full-waveform inversion of crosshole seismic and ground-penetrating radar data in the frequency domain. *Geophysics*, 82(6), H41–H56. https://doi.org/10.1190/geo2016-0008.1

Foti, S., Lai, C. & Lancellotta, R. (2002) Porosity of fluid-saturated porous media from measured seismic wave velocities. *Geotechnique*, 52(5), 359–373. https://doi.org/10.1680/geot.2002.52.5.359

Friedman, S.P. (2005) Soil properties influencing apparent electrical conductivity: a review. *Computers and Electronics in Agriculture*, 46(1-3), 45–70. https://doi.org/10.1016/j.compag.2004.11.001

Gallardo, L.A. & Meju, M.A. (2003) Characterization of heterogeneous near-surface materials by joint 2D inversion of dc resistivity and seismic data. *Geophysical Research Letters*, 30(13), 1658. https://doi.org/10.1029/2003GL017370

Gallardo, L.A. & Meju, M.A. (2004) Joint two-dimensional DC resistivity and seismic travel time inversion with cross-gradients constraints. *Journal of Geophysical Research*, 109(B3), B03311. https://doi.org/10.1029/2003JB002716

Gao, G., Abubakar, A. & Habashy, T. (2012) Joint petrophysical inversion of electromagnetic and full-waveform seismic data. *Geophysics*, 77(3), WA3–WA18. https://doi.org/10.1190/geo2011-0157.1

Garofalo, F., Sauvin, G., Socco, L.V. & Lecomte, I. (2015) Joint inversion of seismic and electrical data applied to 2D media. *Geophysics*, 80(4), EN93–EN104. https://doi.org/10.1190/geo2014-0313.1

Gase, A.C., Bradford, J.H. & Brand, B.D. (2018) Estimation of porosity and water saturation in dual-porosity pyroclastic deposits from joint analysis of compression, shear, and electromagnetic velocities. *Geophysics*, 83(3), ID1–ID11. https://doi.org/10.1190/geo2017-0234.1

Gassmann, F. (1951) Uber die Elastizitat poroser Medien. *Vierteljahrsschrift der Naturforschenden Gesellschaft*, 96, 1–23.

Haber, E. & Oldenburg, D. (1997) Joint inversion: a structural approach. *Inverse Problems*, 13(1), 63–77. https://doi.org/10.1088/0266-5611/13/1/006

Hadamard, J. (1902) Sur les problèmes aux dériveès partielles et leur signification physique. *Princeton University Bulletin*, 13, 49–52.

Haskell, N.A. (1953) The dispersion of surface waves on multilayered media. *Bulletin of the Seismological Society of America*, 43(1), 17–34. https://doi.org/10.1785/BSSA0430010017

Hellman, K., Ronczka, M., Günther, T., Wennermark, M., Rücker, C. & Dahlin, T. (2017) Structurally coupled inversion of ERT and refraction seismic data combined with cluster-based model integration. *Journal of Applied Geophysics*, 143, 169–181. https://doi.org/10.1016/j.jappgeo.2017.06.008

Hofmann, B.A., Sego, D.C. & Robertson, P.K. (2000) In situ ground freezing to obtain undisturbed samples of loose sand. *Journal of Geotechnical and Geoenvironmental Engineering*, 126(11), 979–989. https://doi.org/10.1061/(ASCE)1090-0241(2000)126:11(979)

Hu, W., Abubakar, A. & Habashy, T.M. (2009) Joint electromagnetic and seismic inversion using structural constraints. *Geophysics*, 74(6), R99–R109. https://doi.org/10.1190/1.3246586

Jackson, P.D., Taylor Smith, D. & Stanford, P.N. (1978) Resistivity-porosity-particle shape relationships for marine sands. *Geophysics*, 43(6), 1250–1268. https://doi.org/10.1190/1.1440891

Kennedy, W.D. & Herrick, D.C. (2012) Conductivity models for Archie rocks. *Geophysics*, 77(3), WA109–WA128. https://doi.org/10.1190/geo2011-0297.1

Koefoed, O.C. (1979) *Geosounding principles, 1 - resistivity sounding measurements*. Amsterdam: Elsevier.

Lesmes, D.P. & Friedman, S.P. (2005) Relationships between the electrical and hydrogeological properties of rocks and soils. *Hydrogeophysics, Water Science and Technology Library*. 50, 87–128. https://doi.org/10.1007/1-4020-3102-5_4

Levenberg, K. (1944) A method for the solution of certain nonlinear problems in least squares. *Quarterly of Applied Mathematics*, 2, 164–168.

Marquardt, D.W. (1963) An algorithm for least squares estimation of nonlinear parameters. *Journal of the Society of Industrial Applied Mathematics*, 11(2), 431–441. https://doi.org/10.1137/0111030

Mavko, G., Mukerji, T. & Dvorkin, J. (2009) *The rock physics handbook: tools for seismic analysis of porous media*, 2nd edition. 2, Cambridge: Cambridge University Press.

Moorkamp, M., Heincke, B., Jegen, M., Roberts, A. & Hobbs, R.W. (2011) A framework for 3-D joint inversion of MT, gravity and seismic refraction data. *Geophysical Journal International*, 184(1), 477–493. https://doi.org/10.1111/j.1365-246X.2010.04856.x

Moorkamp, M., Heincke, B., Jegen, M., Hobbs, R.W. & Roberts, A.W. (2016) Joint inversion in hydrocarbon exploration. In: Moorkamp, M., Lelièvre, P. G., Linde, N. & Khan, A. (Eds.) *Integrated imaging of the earth: theory and applications*, 1st edition. Hoboken, NJ: John Wiley & Sons, Inc, pp. 167–189.

Mori, K. & Sakai, K. (2016) The GP sampler: a new innovation in core sampling. *Australian Geomechanics Society*, 51(4), 131–166.

Olsen, P.A. (2011) Coarse-scale resistivity for saturation estimation in heterogeneous reservoirs based on Archie's formula. *Geophysics*, 76(2), E35–E43. https://doi.org/10.1190/1.3541966

Piatti, C., Socco, L.V., Boiero, D. & Foti, S. (2013) Constrained 1D joint inversion of seismic surface waves and P-refraction travel times. *Geophysical Prospecting*, 61(1), 77–93. https://doi.org/10.1111/j.1365-2478.2012.01071.x

Reynolds, J.M. (1997) *An Introduction to Applied and Environmental Geophysics*. 1, Chichester, England: John Wiley and Sons Ltd, 1–712. 978-0-471-48535-3

Ronczka, M., Wisén, R. & Dahlin, T. (2018) Geophysical preinvestigation for a Stockholm tunnel project: joint inversion and interpretation of geoelectric and seismic refraction data in an urban environment. *Near Surface Geophysics*, 16(3), 258–268. https://doi.org/10.3997/1873-0604.2018009

Salem, H.S. (2000) Poisson's ratio and the porosity of surface soils and shallow sediments, determined from seismic compressional and shear wave velocities. *Geotechnique*, 50(4), 461–463. https://doi.org/10.1680/geot.2000.50.4.461

Santamarina, J.C. (2001) *Soils and waves: particulate materials behaviour, characterization and process monitoring*. Hoboken, NJ: Wiley and Sons. ISBN: 978-0-471-49058-6

Senkaya, M., Karsli, H., Socco, L.V. & Foti, S. (2020) Obtaining reliable S-wave velocity depth profile by joint inversion of geophysical data: the combination of active surface-wave, seismic refraction and electric sounding data. *Near Surface Geophysics*, 18, 659–682. https://doi.org/10.1002/nsg.12126

Singh, S., Seed, H.B. & Chan, C. (1982) Undisturbed sampling of saturated sands by freezing. *Journal of Geotechnical and Geoenvironmental Engineering, ASCE*, 108(2), 247–264. https://doi.org/10.1061/AJGEB6.0001242

Socco, L.V., Boiero, D., Foti, S. & Wisén, R. (2009) Laterally constrained inversion of ground roll from seismic reflection records. *Geophysics*, 74, G35–G45. https://doi.org/10.1190/1.3223636

Tarantola, A. (1987) *Inverse problem theory: methods for data fitting and model parameter estimation*. Amsterdam: Elsevier Science Publisher.

Thomson, W.T. (1950) Transmission of elastic waves through a stratified solid medium. *Journal of Applied Physics*, 21, 89–93. https://doi.org/10.1063/1.1699629

Toksöz, M.N., Cheng, C.H. & Timur, A. (1976) Velocities of seismic waves in porous rocks. *Geophysics*, 41(4), 621–645. https://doi.org/10.1190/1.1440639

Viezzoli, A., Christiansen, A.V., Auken, E. & Sørensen, K. (2008) Quasi-3D modeling of airborne TEM data by spatially constrained inversion. *Geophysics*, 73(3), F105–F113. https://doi.org/10.1190/1.2895521

Waxman, M.H. & Smits, L.J.M. (1968) Electrical conductivities in oil-bearing shaly sand. *Society of Petroleum Engineering Journal*, 8(2), 107–122. https://doi.org/10.2118/1863-A

Wyllie, M.R.J., Gregory, A.R. & Gardner, G.H.F. (1956) Elastic wave velocities in heterogeneous and porous media. *Geophysics*, 21(1), 41–70. https://doi.org/10.1190/1.1438217

Wyllie, M.R.J., Gregory, A.R. & Gardner, G.H.F. (1958) An experimental investigation of factors affecting elastic wave velocities in porous media. *Geophysics*, 23(3), 459–493. https://doi.org/10.1190/1.1438493